

Yang Monopoles and Emergent Three-Dimensional Topological Defects in Interacting Bosons

Yangqian Yan and Qi Zhou

Department of Physics and Astronomy, Purdue University, West Lafayette, Indiana 47906, USA



(Received 24 October 2017; published 8 June 2018)

The Yang monopole as a zero-dimensional topological defect has been well established in multiple fields in physics. However, it remains an intriguing question to understand the interaction effects on Yang monopoles. Here, we show that the collective motion of many interacting bosons gives rise to exotic topological defects that are distinct from Yang monopoles seen by a single particle. Whereas interactions may distribute Yang monopoles in the parameter space or glue them to a single giant one of multiple charges, three-dimensional topological defects also arise from continuous manifolds of degenerate many-body eigenstates. Their projections in lower dimensions lead to knotted nodal lines and nodal rings. Our results suggest that ultracold bosonic atoms can be used to create emergent topological defects and directly measure topological invariants that are not easy to access in solids.

DOI: [10.1103/PhysRevLett.120.235302](https://doi.org/10.1103/PhysRevLett.120.235302)

Yang monopoles play a crucial role in non-Abelian gauge theories and have influential impacts in multiple subareas of physics [1]. In high energy physics, they lay the foundation of Yang-Mills theory and the standard model [2–6]. In condensed matter physics, they give rise to nontrivial topological quantum states characterized by the second Chern number, C_2 [7–9]. In a five-dimensional (5D) parameter space, a Yang monopole represents a zero-dimensional point defect with a fourfold degeneracy. Away from a Yang monopole, a spin-3/2 or pseudospin-3/2 could see such a point topological defect from either local non-Abelian Berry curvatures or C_2 . When a four-dimensional (4D) surface encloses the Yang monopole, $C_2 = 1$. One could view a Yang monopole as a magnetic monopole of “charge” 1.

Whereas Yang monopoles remained a theoretical concept for decades, Sugawa *et al.* at the National Institute of Standards and Technology (Gaithersburg, MD) (NIST) delivered a Yang monopole for the first time in laboratories by engineering the couplings among four hyperfine spin states of ultracold bosonic atoms [10]. Each boson in this experiment represents a pseudospin-3/2. While many experiments have used bosons to probe local Abelian Berry curvatures [11–13], C_2 has been extracted in the NIST experiment by integrating the non-Abelian Berry curvature on 4D surfaces. Very recently, C_2 has also been measured in optical lattices and photonic crystals [14,15].

Though Yang monopoles have been well established in noninteracting systems, a fundamental question remains. Are topological defects seen by a collection of many interacting spin-3/2 s the same as those seen by each individual one? In this Letter, we show that the interactions allow physicists to access completely different topological

defects arising from collective motions of many particles. These emergent topological defects signify the vital importance of interactions on Yang monopoles, and they demonstrate the power of ultracold atoms in creating and detecting novel topological phenomena that are not easy to access in solids.

Our main results are summarized as follows. For odd particle numbers N , repulsive interactions distribute Yang monopoles on a quantization axis in the parameter space, and attractive interactions glue them to a single one of “charge” N^2 at the origin. In contrast, for $N = 4n + 2$, where n is a non-negative integer, interactions produce multiple three-dimensional (3D) topological defects. When $N = 4n$, the many-body ground state is unique for repulsive interactions, and no topological defect can be seen by the ground state. The results of attractive interactions are similar to those for $N = 4n + 2$. Here, 3D defects emerge purely from interaction effects in bosons, unlike those studied in noninteracting electronic systems [16–20]. We also show how to use ultracold bosons to directly measure the topological invariants in laboratories.

Our work was motivated by a recent paper by Ho and Li [21]. Based on a mean field approach, this pioneering work shows that a Yang monopole may be stretched into an extended manifold due to interactions. In this mean field approach, all pseudospin-3/2 s are described by the same condensate wave function. Here, we provide an exact solution for a generic N pseudospin-3/2 system. We show that the many-body ground state becomes degenerate in certain locations in the parameter space. These degenerate many-body eigenstates give rise to novel topological defects beyond mean field predictions.

Hamiltonian.—The single-particle Hamiltonian that describes a Yang monopole reads [20,21]

$$\hat{K} = -R_z \tau_z \otimes \hat{n} \cdot \vec{\sigma} - R_x \tau_x - R_y \tau_y, \quad (1)$$

where $\vec{\sigma}$ and $\vec{\tau}$ are two spin-1/2 operators, and \hat{n} is a unit vector. A single-mode approximation has been taken for the orbital part of the wave function; i.e., bosons share the same spatial wave function. Equation (1), defined in a 5D parameter space, $\mathbf{R} = (R_x, R_y, R_z n_x, R_z n_y, R_z n_z)$, describes a spin-3/2 particle. In the NIST experiment, the first (second) two parameters are determined by the intensities and phases of radio-frequency (microwave) coupling and the last one, $R_z n_z$, is adjusted by the detuning [10]. For convenience for later discussions, we rewrite this Hamiltonian,

$$\hat{K} = \sum_{i=1}^4 \epsilon_i \hat{a}_i^\dagger \hat{a}_i + \sum_{j=2}^4 \sum_{i=1}^{j-1} (t_{ij} \hat{a}_i^\dagger \hat{a}_j + \text{H.c.}), \quad (2)$$

which describes four lattice sites coupled by certain intersite tunnelings t_{ij} , as shown in Fig. 1(a). \hat{a}_i^\dagger (\hat{a}_i) is the creation (annihilation) operator at site i . ϵ_i is the on-site energy, $-\epsilon_1 = \epsilon_2 = \epsilon_3 = -\epsilon_4 = R_z n_z$, $t_{13} = t_{24} = -R_x + iR_y$, $t_{12} = -t_{34} = -R_z n_x + iR_z n_y$, and $t_{14} = t_{23} = 0$. The 5D parameter space is now spanned by the complex tunnelings t_{12} and t_{13} , and $R_z n_z$ that determine the on-site energies. As this pseudospin-3/2 Hamiltonian respects time reversal

symmetry, every eigenstate is doubly degenerate, consistent with Kramers theorem. For many-body systems, we consider the Hamiltonian,

$$\hat{H} = \hat{K} + \hat{U}, \quad \hat{U} = g \sum_{i=1}^4 (\hat{a}_i^\dagger a_i)^2 = g \sum_{i=1}^4 n_i^2, \quad (3)$$

where g is the on-site interaction strength. n_i represents the occupation in the i th lattice site and $\sum_{i=1}^4 n_i = N$ is satisfied. Because \hat{U} respects the time reversal symmetry, for odd N , the Kramers theorem still applies. Though interspin interactions exist in the NIST experiment, here, we concretize the discussions on intraspin interactions, which correspond to on-site interactions in Eq. (3), to reveal fundamental interaction effects on Yang monopoles. A Yang monopole may also be realized alternatively using coupled four lattice sites described by Eq. (2) [22]. It is then natural to consider \hat{H} in Eq. (3) as on-site interactions dominate.

We solve \hat{H} exactly and obtain the many-body eigenstates $|\Psi_m\rangle$ for N bosons. $|\Psi_m\rangle$ is expanded using Fock states, $|\Psi_m\rangle = \sum_{\{n_i\}} \alpha_m \{n_i\} |n_1, n_2, n_3, n_4\rangle$. When nodal points are observed, we compute C_2 [5,6,22],

$$C_2 = \frac{1}{32\pi^2} \int_{S^4} d\mathbf{R} \epsilon_{\mu\nu\rho\lambda} (\text{Tr}[F_{\mu\nu} F_{\rho\lambda}] - \text{Tr}[F_{\mu\nu}] \text{Tr}[F_{\rho\lambda}]), \quad (4)$$

where $F_{\mu\nu} = \partial_\mu A_\nu - \partial_\nu A_\mu + i[A_\mu, A_\nu]$, $A_\nu^{mn} = -i\langle \Psi_m | \partial_\nu | \Psi_n \rangle$. Matrix $F_{\mu\nu}$ and A_μ are the non-Abelian Berry curvature and the non-Abelian Berry connection for the ground state manifold, respectively. S^4 is a closed 4D surface in the parameter space, and $\epsilon_{\mu\nu\rho\lambda}$ is Levi-Civita symbol. When nodal lines or rings are observed, corresponding topological invariants are computed.

Away from the origin of the parameter space, the single-particle ground state becomes twofold degenerate. Thus, for N non-interacting bosons, there are $N + 1$ degenerate ground states, and C_2 reads $N(N + 1)(N + 2)/6$ [22]. Turning on interactions, results become completely different.

N Yang monopoles.—When $g > 0$, there are N points on the R_5 axis, where the many-body ground state becomes four-fold degenerate. At the origin, $\hat{K} = 0$, there are four ways to distribute $N \in \text{odd}$ bosons in four equivalent lattice sites to minimize the interaction energy, as shown in Figs. 1(b)–1(c). Away from the origin, fourfold degenerate points also exist on the R_5 axis. All tunnelings in Eq. (2) vanish on this axis, as $R_{i \neq 5} = 0$. Many-body eigenstates are simply Fock states. The mismatch of on-site energies $\epsilon_1 - \epsilon_2 = \epsilon_4 - \epsilon_3$ could exactly compensate the penalty of interaction energy for moving one boson from one lattice site to another. For example, for $N = 3$ and $R_5 = g$, states $|1, 1, 0, 1\rangle$, $|1, 0, 1, 1\rangle$, $|2, 0, 0, 1\rangle$, and $|1, 0, 0, 2\rangle$ become degenerate. For any N , the separation between the two nearest points is given by $\Delta R_5 = g$.

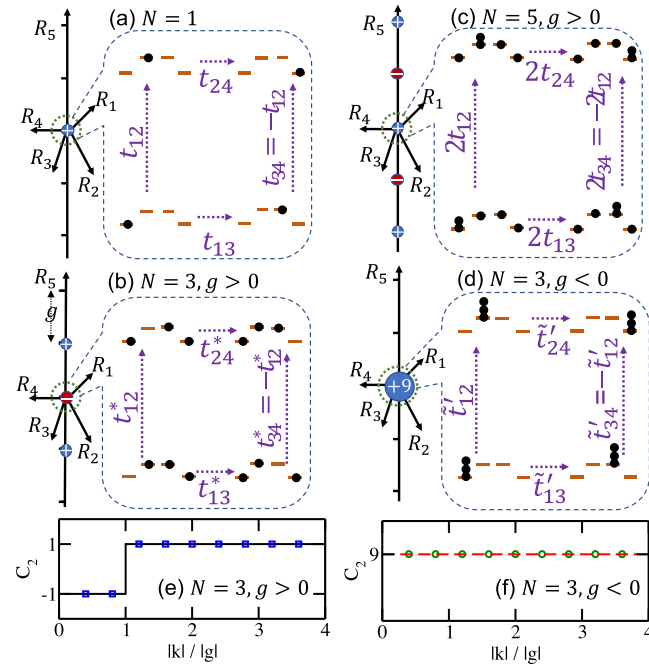


FIG. 1. Yang monopoles for odd N . Blue (red) spheres show the positively (negatively) charged monopoles with charges denoted. (a)–(c), $g > 0$, $N = 1, 3, 5$. (d) $g < 0$, $N = 3$. Insets illustrate effective Hamiltonians near the origin. Orange solid lines (black dots) represent single particle states (bosons). Dotted arrows show effective couplings. (e)–(f) C_2 as a function of the radius $|k|$ of the 5D sphere for three particles. Solid and dashed lines (squares and circles) are analytical (numerical) results.

Away from these fourfold degenerate points, the four Fock states are no longer degenerate, and tunnelings become finite. In the vicinity of each degenerate point, we construct an effective model using the four nearly degenerate states as the basis. Such an effective model has exactly the same formula as the single-particle Hamiltonian in Eq. (2), except that ϵ_i and t_{ij} are modified. We show, e.g., the effective Hamiltonian near the origin, in which the parameters read

$$\tilde{\epsilon}_i = (-1)^{\frac{N-1}{2}} \epsilon_i, \quad \tilde{t}_{ij} = \begin{cases} t_{ij}(N+3)/4 & \text{for } N = 1, 5, \dots \\ t_{ij}^*(N+1)/4 & \text{for } N = 3, 7, \dots \end{cases} \quad (5)$$

Thus, we conclude that each fourfold degenerate point corresponds to a Yang monopole. A subtle difference between $N = 1, 5, \dots$ and $N = 3, 7, \dots$ exists. As shown in Figs. 1(b)–1(c), it is a particle and a hole that tunnel in the effective Hamiltonian for these two cases, respectively. The “charge” of the Yang monopole at the origin for $N = 1, 5, \dots$ is 1 and that for $N = 3, 7, \dots$ is -1 . Similarly, for a fixed N , with increasing distance from the origin, the “charges” of monopoles alternate [22]. When all monopoles are enclosed, $C_2 = 1$.

A giant Yang monopole.—For attractive interactions, only one monopole exists in the parameter space, and its “charge” is N^2 . At the origin, $|N, 0, 0, 0\rangle$, $|0, N, 0, 0\rangle$, $|0, 0, N, 0\rangle$, $|0, 0, 0, N\rangle$ are the four degenerate many-body ground states, as all bosons prefer to occupy the same lattice site to minimize the interaction energy. Away from the origin, an effective model, which has the same formula as Eq. (2), can be constructed. Since a single-particle tunneling t_{ij} moves one boson from one lattice site to another, it requires N steps of single-particle tunneling to couple these states. The parameters in the effective Hamiltonian read

$$\tilde{\epsilon}'_i = N\epsilon_i \quad \text{and} \quad \tilde{t}'_{ij} = c_N t_{ij}^N / g^{N-1}, \quad (6)$$

where c_N is a function of N [22]. Using this effective model, we obtain that the “charge” of the monopole is N^2 [Fig. 1(d)]. The superposition of the four Fock states actually forms a Schrödinger cat state [28–31]. Though not stable for large N , in a few-body system [32,33], a small cat could exist in laboratories such that a Yang monopole of “charge” N^2 is observable.

C_2 for any closed surface is equal to the total “charge” of the monopoles it encloses. If a smooth deformation of the surface does not touch a Yang monopole, C_2 remains unchanged. We numerically calculate C_2 of three particles on a 4D sphere as a function of the radius of the sphere. Figures 1(e)–1(f) show that C_2 is indeed given by the total “charge” of the monopole enclosed in the sphere. Note that, C_2 is much smaller than that of noninteracting systems.

This is because an infinitesimal interaction reduces the $N + 1$ fold degeneracy of noninteracting systems to a twofold one. Nevertheless, we have verified that, the total C_2 of the lowest $N + 1$ bands for weakly interacting systems is indeed the same as that for the corresponding noninteracting systems.

3D topological defects.—If the average particle number per site is an integer, i.e., $N = 4n$, where n is a positive integer, the many-body ground state becomes unique for $g > 0$. This is best understood in the strongly interacting regime. As bosons prefer to distribute evenly in the four lattice sites to minimize the interaction energy, the unique ground state cannot see any topological defects. When $g < 0$, the many-body ground state is fourfold degenerate at the origin of the parameter space, similar to the case of odd particles. Away from the origin, an effective Hamiltonian can be constructed in the same manner. However, the resultant effective Hamiltonian is distinct. The effective coupling between the Fock states, such as $|N, 0, 0, 0\rangle$ and $|0, N, 0, 0\rangle$, now requires an even number steps of single-particle tunnelings. In the single-particle Hamiltonian in Eq. (2), t_{12} and t_{34} have different signs. This minus sign remains unchanged in the effective model for odd N , as both effective couplings, \tilde{t}'_{12} and \tilde{t}'_{34} , are proportional to odd powers of t_{12} and t_{34} .

For even particle numbers, the minus sign disappears. Completely different topological defects arise. The effective Hamiltonian reads

$$\hat{H}_{\text{eff}} = a\tilde{\tau}_z \otimes \tilde{\sigma}_z + b\tilde{\tau}_x \otimes I + c\tilde{\tau}_y \otimes I + dI \otimes \tilde{\sigma}_x + eI \otimes \tilde{\sigma}_y, \quad (7)$$

where $a = -2R_5$, $b = -(R_1^2 - R_2^2)/g$, $c = -2R_1R_2/g$, $d = -(R_3^2 - R_4^2)/g$, and $e = -2R_3R_4/g$ for $N = 2$. $\tilde{\sigma}$ and $\tilde{\tau}$ are two spin-1/2 s, and I is the identity matrix. The eigenstates of $\tilde{\tau}_z \otimes \tilde{\sigma}_z$, $|\uparrow\uparrow\rangle$, $|\uparrow\downarrow\rangle$, $|\downarrow\uparrow\rangle$, $|\downarrow\downarrow\rangle$, correspond to $|N, 0, 0, 0\rangle$, $|0, N, 0, 0\rangle$, $|0, 0, N, 0\rangle$, $|0, 0, 0, N\rangle$. The eigenenergy of \hat{H}_{eff} reads

$$E = \pm \sqrt{a^2 + \left(\sqrt{b^2 + c^2} \pm \sqrt{d^2 + e^2} \right)^2}, \quad (8)$$

which shows that eigenstates become degenerate in certain 3D continuous manifolds.

$\{\mathcal{M}_1 : R_1 = R_2 = 0\}$ and $\{\mathcal{M}'_1 : R_3 = R_4 = 0\}$, both the ground and excited states, are doubly degenerate.

$\{\mathcal{M}_2 : R_5 = 0, R_1^2 + R_2^2 = R_3^2 + R_4^2\}$, the second and third states are degenerate, and the ground state (the fourth state) is unique.

As Kramers theorem does not apply to an even number of spin-3/2 s, the evenfold degeneracy is not guaranteed, and \mathcal{M}_2 is possible here. These three manifolds intersect at the origin of the 5D parameter space. Away from them, there is no degeneracy. \mathcal{M}_2 signifies the vanishing gap

between the lowest and the highest two states on any closed 4D surface. Thus, C_2 is no longer appropriate to characterize the topological defects. Each manifold is characterized by its own corresponding topological invariant. Meanwhile, the projections of them in lower dimensions lead to knotted nodal lines and rings.

Since \mathcal{M}_1 and \mathcal{M}_2 are 3D defects in a 5D parameter space, a one-dimensional (1D) loop can be defined without intersecting them. We calculate the Berry phase $\gamma_m = -i \oint_M d\mathbf{R} \cdot \langle \Psi_m | \nabla_{\mathbf{R}} | \Psi_m \rangle$ for the m th eigenstate $|\Psi_m\rangle$, where M denotes a closed loop in the parameter space. For any loop that does not interlock the defects, i.e., a loop that can shrink to a single point without closing the gap, $\gamma_m = 0$. For a loop interlocking the defects, $\gamma_1 + \gamma_2 = 0$ or π (or their multiples). This defines a Z_2 index ζ_1 for the defects [19]. For M_1 and M_1' , we find that $\gamma = N\pi$ for all eigenstates and $\zeta_1 = 0$. For M_2 , we find that $\gamma = (0, \pi, \pi, 0)$ for each eigenstate and $\zeta_1 = 1$.

To better visualize this Z_2 invariant, we project $\mathcal{M}_1, \mathcal{M}_1'$, and \mathcal{M}_2 to lower dimensions, i.e., reducing the dimension by fixing the values of certain parameters. Defining $\vec{m} = (d, e)$ and $|\vec{m}| = \sqrt{d^2 + e^2} = (R_3^2 + R_4^2)/|g|$, the eigenenergies in Eq. (8) read $E = \pm \sqrt{a^2 + (\sqrt{b^2 + c^2} \pm |\vec{m}|)^2}$. Interestingly, this energy spectrum is identical to the one used to study nodal rings in electronic systems [19]. As shown in Fig. 2, for any finite $|\vec{m}|$, \mathcal{M}_1 becomes an infinite nodal line, and \mathcal{M}_2 becomes a nodal ring with radius $|\vec{m}|$. \mathcal{M}_1' does not show up in this subspace. The dashed circles that interlock the nodal ring or line allow one to compute γ . Decreasing $|\vec{m}|$, the nodal ring shrinks, and the nodal line remains unchanged. When $|\vec{m}| = 0$, the nodal ring reduces to a single point at the origin, and the gap does not open. In particular, this whole 3D subspace precisely becomes \mathcal{M}_1' , and the eigenenergies are twofold degenerate everywhere. For this particular set of parameters, \hat{H}_{eff} describes a quantum spin Hall effect, as

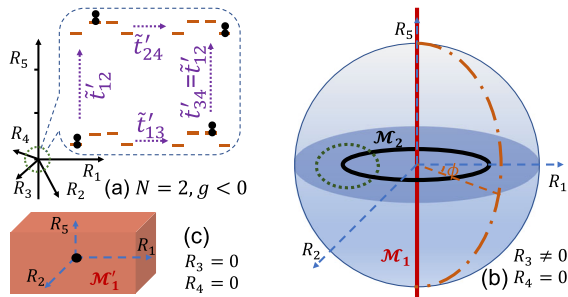


FIG. 2. (a) The effective Hamiltonian for two particles with $g < 0$. (b)–(c) shows the projections of the defects in a 3D subspace with a fixed R_3 and R_4 . (b) The red line (black ring) shows the projection of \mathcal{M}_1 (\mathcal{M}_2). The green dotted circle (blue 2D sphere) is used to calculate ζ_1 (ζ_2). The dash-dotted longitude line connecting the north and south poles defines a ϕ -dependent Wilson line. (c) When \mathcal{M}_2 reduces to a point at the origin, \mathcal{M}_1' occupies the entire 3D subspace (red box).

$\sigma_z = \pm 1$ corresponds to two opposite effective magnetic fields acting on $\vec{\tau}$. When \vec{m} changes sign, the nodal ring appears again.

On any two-dimensional (2D) sphere that does not touch \mathcal{M}_2 , the lowest two eigenstates are separated from the rest. On such a sphere, the projection to the lowest k states, which are separated from the higher l states, establishes another topological invariant, ζ_2 , of the nodal ring [19,34]. To be explicit, Wilson lines connecting the north and south pole along a half longitude depend on the polar angle ϕ , as shown in Fig. (2). Such ϕ dependence allows one to define a winding number n_w . For generic $k, l > 2$, $\zeta_2 = \text{mod}(n_w, 2)$ defines a Z_2 index. In our system, $k = 2$, and the winding number becomes a Z index [19,35]. For our effective model \hat{H}_{eff} , we find that $\zeta_2 = 1$ for any 2D sphere that encloses the nodal ring; otherwise, $\zeta_2 = 0$. Thus, the nodal ring defines a topological phase transition where ζ_2 changes its value. For repulsive interactions, M_1 and M_1' switch with M_2 [22]. While the topological defects are derived in the strongly interacting regime, we numerically verified that they hold even for weakly interacting systems.

Realizations in few-body systems.—With increasing N , the energy splitting between eigenstates decreases. Moreover, due to the small scattering length a_s and the extended orbital wave function in the NIST experiment, the interaction strength g is very weak. For instance, for $a_s = 5$ nm, $N = 10^5$, the trapping frequency $\omega = 2\pi * 70$ Hz, and $g \approx 0.04$ Hz, which is too weak to have significant effects. The main experimental results are well explained by non-interacting pictures. Thus, to better resolve these topological defects and the associated topological invariants, experimentalists could use few-body systems to reduce N and increase g .

A 2D optical superlattice is a promising platform to realize Hamiltonians in Eqs. (3) and (7) in the real space. Such a superlattice divides the system into many isolated plaquettes, each of which contains four sites. Currently available experimental techniques allow experimentalists to dress and detect each individual plaque. Many interesting few-body phenomena have been explored [36–38]. Using laser-assisted tunneling and a magnetic field gradient, both the amplitude and phase of the tunnelings can be engineered [37,39]. The on-site potential can be tuned by superposing an additional 1D lattice tilted by 45° . The Hamiltonian in Eq. (1) can then be delivered. Turning on interactions, the effective Hamiltonian in Eq. (7) could then be explored. For instance, the interaction strength is around 100 Hz for Rb in optical lattices with laser wavelength of 767 nm and depth of $8E_R$, where E_R is the characteristic energy scale defined by the wavelength. Increasing the lattice depth or the scattering length, g can be further enhanced. Using realistic experimental parameters, we find that the previously discussed topological defects can indeed be resolved [22]. Experimentalists can also realize Eq. (7) directly in noninteracting systems by engineering the

intersite couplings. A few other approaches, including mesoscopic traps, optical tweezers, ion traps, and superconducting circuits, can also be used to study few-body physics related to our work [22,32,33].

A unique advantage of ultracold atoms is that the topological defects and the associated topological invariants can be directly probed. To measure ζ_1 , the local Berry curvature could be measured to extract the Berry phase accumulated in a 1D loop [10,11,40–44]. To measure ζ_2 , Wilson lines can be measured in the same manner in Ref. [45].

In the NIST experiment on spinor Bose-Einstein condensates, interspin interactions exist. Thus, we need to consider generic interactions $\sum_i g_i n_i^2 + \sum_{i<j} g_{ij} n_i n_j$, where g_i (g_{ij}) is the intraspin (interspin) interaction strength. If such interactions preserve time reversal symmetry, our main results remain unchanged. For interactions that break time reversal symmetry, even richer physics regarding topological defects arise [22].

In conclusion, we have shown that interactions give rise to emergent topological defects distinct from those seen by each individual particle. Depending on the total particle number and the interaction strength, either giant Yang monopoles of multiple charges or 3D continuous topological defects emerge. Such topological defects can be accessed in current experiments, in particular, those on few-body systems. While Dirac monopoles control many 2D and 3D topological matters, Yang monopoles and C_2 are crucial for topological quantum phenomena in high dimensions, including 4D quantum Hall effects. Nodal lines and nodal rings as continuous topological defects also provide physicists unprecedented topological quantum matter. We hope that our work will stimulate more studies on using ultracold atoms to create and measure topological defects in high dimensional interacting systems.

Q. Z. acknowledges useful discussions with T. L. Ho, I. Spielman, S. Sugawa, and C. Fang. Y. Y. acknowledges useful discussions with C. Li. This work is supported by startup funds from Purdue University.

-
- [1] C. N. Yang and R. L. Mills, Conservation of isotopic spin and isotopic gauge invariance, *Phys. Rev.* **96**, 191 (1954).
 - [2] C. N. Yang, Generalization of Dirac's monopole to SU_2 gauge fields, *J. Math. Phys. (N.Y.)* **19**, 320 (1978).
 - [3] G. 't Hooft, The standard model of particle physics, *Nature (London)* **448**, 271 (2007).
 - [4] G. 't Hooft, Magnetic monopoles in unified gauge theories, *Nucl. Phys. B* **79**, 276 (1974).
 - [5] S.-S. Chern, Characteristic classes of Hermitian manifolds, *Ann. Math.* **47**, 85 (1946).
 - [6] S. Chern, *Topics in Differential Geometry* (The Institute for Advanced Study, Princeton, 1951).
 - [7] C.-H. Chern, H.-D. Chen, C. Wu, J.-P. Hu, and S.-C. Zhang, Non-Abelian Berry phase and Chern numbers in higher spin-pairing condensates, *Phys. Rev. B* **69**, 214512 (2004).

- [8] D. Xiao, J. Shi, D. P. Clougherty, and Q. Niu, Theory of electric polarization induced by inhomogeneity in crystals, [arXiv:0711.1855](https://arxiv.org/abs/0711.1855).
- [9] X.-L. Qi, T. L. Hughes, and S.-C. Zhang, Topological field theory of time-reversal invariant insulators, *Phys. Rev. B* **78**, 195424 (2008).
- [10] S. Sugawa, F. Salces-Carcoba, A. R. Perry, Y. Yue, and I. B. Spielman, Observation of a non-Abelian Yang monopole: From new Chern numbers to a topological transition, [arXiv:1610.06228](https://arxiv.org/abs/1610.06228).
- [11] M. Atala, M. Aidelsburger, J. T. Barreiro, D. Abanin, T. Kitagawa, E. Demler, and I. Bloch, Direct measurement of the Zak phase in topological Bloch bands, *Nat. Phys.* **9**, 795 (2013).
- [12] M. Aidelsburger, M. Lohse, C. Schweizer, M. Atala, J. T. Barreiro, S. Nascimbène, N. R. Cooper, I. Bloch, and N. Goldman, Measuring the Chern number of Hofstadter bands with ultracold bosonic atoms, *Nat. Phys.* **11**, 162 (2015).
- [13] M. Lohse, C. Schweizer, O. Zilberberg, M. Aidelsburger, and I. Bloch, A Thouless quantum pump with ultracold bosonic atoms in an optical superlattice, *Nat. Phys.* **12**, 350 (2016).
- [14] M. Lohse, C. Schweizer, H. M. Price, O. Zilberberg, and I. Bloch, Exploring 4D quantum Hall physics with a 2D topological charge pump, *Nature (London)* **553**, 55 (2018).
- [15] O. Zilberberg, S. Huang, J. Guglielmon, M. Wang, K. Chen, Y. E. Kraus, and M. C. Rechtsman, Photonic topological boundary pumping as a probe of 4D quantum Hall system, *Nature (London)* **553**, 59 (2018).
- [16] A. A. Burkov, M. D. Hook, and L. Balents, Topological nodal semimetals, *Phys. Rev. B* **84**, 235126 (2011).
- [17] A. P. Schnyder, P. M. R. Brydon, and C. Timm, Types of topological surface states in nodal noncentrosymmetric superconductors, *Phys. Rev. B* **85**, 024522 (2012).
- [18] P. Hosur, X. Dai, Z. Fang, and X.-L. Qi, Time-reversal-invariant topological superconductivity in doped Weyl semimetals, *Phys. Rev. B* **90**, 045130 (2014).
- [19] C. Fang, Y. Chen, H.-Y. Kee, and L. Fu, Topological nodal line semimetals with and without spin-orbital coupling, *Phys. Rev. B* **92**, 081201 (2015).
- [20] B. Lian and S.-C. Zhang, Five-dimensional generalization of the topological Weyl semimetal, *Phys. Rev. B* **94**, 041105 (2016).
- [21] T.-L. Ho and C. Li, The Chern Numbers of Interaction-stretched Monopoles in Spinor Bose Condensates, [arXiv:1704.03833](https://arxiv.org/abs/1704.03833).
- [22] See Supplemental Material at <http://link.aps.org/supplemental/10.1103/PhysRevLett.120.235302>, which includes Refs. [23–27], for detailed derivations of noninteracting C_2 , the location and “charge” of the Yang monopole for odd N and positive g , C_2 for odd N , the expression for c_N , topological invariants, 3D topological defects for even number of particles with repulsive interaction, linking number, experimental schemes for exploring few-body physics, and generic interactions.
- [23] G. Jotzu, M. Messer, R. Desbuquois, M. Lebrat, T. Uehlinger, D. Greif, and T. Esslinger, Experimental realization of the topological Haldane model with ultracold fermions, *Nature (London)* **515**, 237 (2014).

- [24] C. V. Parker, L.-C. Ha, and C. Chin, Direct observation of effective ferromagnetic domains of cold atoms in a shaken optical lattice, *Nat. Phys.* **9**, 769 (2013).
- [25] A. Kaufman, B. Lester, M. Foss-Feig, M. Wall, A. Rey, and C. Regal, Entangling two transportable neutral atoms via local spin exchange, *Nature (London)* **527**, 208 (2015).
- [26] P. Roushan, C. Neill, Y. Chen, M. Kolodrubetz, C. Quintana, N. Leung, M. Fang, R. Barends, B. Campbell, Z. Chen *et al.*, Observation of topological transitions in interacting quantum circuits, *Nature (London)* **515**, 241 (2014).
- [27] M. D. Schroer, M. H. Kolodrubetz, W. F. Kindel, M. Sandberg, J. Gao, M. R. Vissers, D. P. Pappas, A. Polkovnikov, and K. W. Lehnert, Measuring a Topological Transition in an Artificial Spin-1/2 System, *Phys. Rev. Lett.* **113**, 050402 (2014).
- [28] W. H. Zurek, Decoherence and the transition from quantum to classical, *Phys. Today* **44**, 36 (1991).
- [29] C. Monroe, D. M. Meekhof, B. E. King, and D. J. Wineland, A “Schrodinger Cat” superposition state of an atom, *Science* **272**, 1131 (1996).
- [30] T.-L. Ho and C. V. Ciobanu, The Schrödinger cat family in attractive Bose gases, *J. Low Temp. Phys.* **135**, 257 (2004).
- [31] E. J. Mueller, T.-L. Ho, M. Ueda, and G. Baym, Fragmentation of Bose-Einstein condensates, *Phys. Rev. A* **74**, 033612 (2006).
- [32] A. N. Wenz, G. Zürn, S. Murmann, I. Brouzos, T. Lompe, and S. Jochim, From few to many: Observing the formation of a Fermi sea one atom at a time, *Science* **342**, 457 (2013).
- [33] G. Zürn, A. N. Wenz, S. Murmann, A. Bergschneider, T. Lompe, and S. Jochim, Pairing in Few-Fermion Systems with Attractive Interactions, *Phys. Rev. Lett.* **111**, 175302 (2013).
- [34] A. Hatcher, *Algebraic Topology* (Cambridge University Press, Cambridge, UK, 2002).
- [35] C. Fang and H. Weng and X. Dai and Z. Fang, Topological nodal line semimetals, *Chin. Phys. B* **25**, 117106 (2016).
- [36] S. Nascimbène, Y.-A. Chen, M. Atala, M. Aidelsburger, S. Trotzky, B. Paredes, and I. Bloch, Experimental Realization of Plaquette Resonating Valence-Bond States with Ultracold Atoms in Optical Superlattices, *Phys. Rev. Lett.* **108**, 205301 (2012).
- [37] M. Aidelsburger, M. Atala, M. Lohse, J. T. Barreiro, B. Paredes, and I. Bloch, Realization of the Hofstadter Hamiltonian with Ultracold Atoms in Optical Lattices, *Phys. Rev. Lett.* **111**, 185301 (2013).
- [38] H.-N. Dai, B. Yang, A. Reingruber, H. Sun, X.-F. Xu, Y.-A. Chen, Z.-S. Yuan, and J.-W. Pan, Four-body ring-exchange interactions and anyonic statistics within a minimal toric-code Hamiltonian, *Nat. Phys.* **13**, 1195 (2017).
- [39] H. Miyake, G. A. Siviloglou, C. J. Kennedy, W. C. Burton, and W. Ketterle, Realizing the Harper Hamiltonian with Laser-Assisted Tunneling in Optical Lattices, *Phys. Rev. Lett.* **111**, 185302 (2013).
- [40] V. Gritsev and A. Polkovnikov, Dynamical quantum hall effect in the parameter space, *Proc. Natl. Acad. Sci. U.S.A.* **109**, 6457 (2012).
- [41] H. M. Price and N. R. Cooper, Mapping the Berry curvature from semiclassical dynamics in optical lattices, *Phys. Rev. A* **85**, 033620 (2012).
- [42] P. Hauke, M. Lewenstein, and A. Eckardt, Tomography of Band Insulators from Quench Dynamics, *Phys. Rev. Lett.* **113**, 045303 (2014).
- [43] L. Duca, T. Li, M. Reitter, I. Bloch, M. Schleier-Smith, and U. Schneider, An Aharonov-Bohm interferometer for determining Bloch band topology, *Science* **347**, 288 (2015).
- [44] M. Kolodrubetz, Measuring the Second Chern Number from Nonadiabatic Effects, *Phys. Rev. Lett.* **117**, 015301 (2016).
- [45] T. Li, L. Duca, M. Reitter, F. Grusdt, E. Demler, M. Endres, M. Schleier-Smith, I. Bloch, and U. Schneider, Bloch state tomography using Wilson lines, *Science* **352**, 1094 (2016).